Section X2:
Design of a trussed wing structure

This example is freely inspired from Bruhn's book. It provides a "before-computer-age" approach to the computation of a three-dimensional fully-trussed wing structure. While such a computation could be done with a 3D finite-element truss solver package, a fully numerical approach lacks the flexibility of changing parameters typically associated with a design phase. Additionally, the fully analytical approach forces to think deeply about forces, reactions, internals versus externals, and greatly improves the understanding of load path distribution in structures. Reviewing such an "old-school approach" is therefore of considerable pedagogical interest. Furthermore, the results can be put in spreadsheet form to speed up calculations, allow variation of parameters or perform inverse computations.

1 Scope of the problem

Let us assume a redesign of a Piper Cub type aeroplane. This aeroplane is shown on figure X2–1. It was a very successful general aviation aircraft originally designed in the 1930's and still largely flown today, sometimes compared to the Ford-T of aviation [1,2]. The "Super Cub" was designed in 1949 from the earlier "Cub" design and was built in many versions until 1994.

Figure X2–1 Piper PA18 "Super Cub" flown by the author as a student pilot

The aircraft has a fully "truss-and-cloth" structure. The wing details are shown on figure X2–2. It shows an internal skeleton made of two main spars fixed in the vertical direction but pinned (free to rotate) in the wing plane. They are held in position through supporting struts, probably connected to the spars between WBL 132.50 and 138.63. The figure shows the crossed wires making up the diagonal members of the "drag truss" (the triangulated truss in the plane of the wing). Only the inboard truss cell uses a rigid diagonal member, with additional support for the wing fuel tank. The ribs are not supposed to play a major structural role. The outer circular fairing which ends the wing is not supposed to be load-resistant either (except for the localised suction due to local pressure forces).

Our design will be based on a four-cell fully-wired plane truss supported by two struts. The global dimensions are those of the PA-18: a chord of 66 inches and a span of 35 feet.

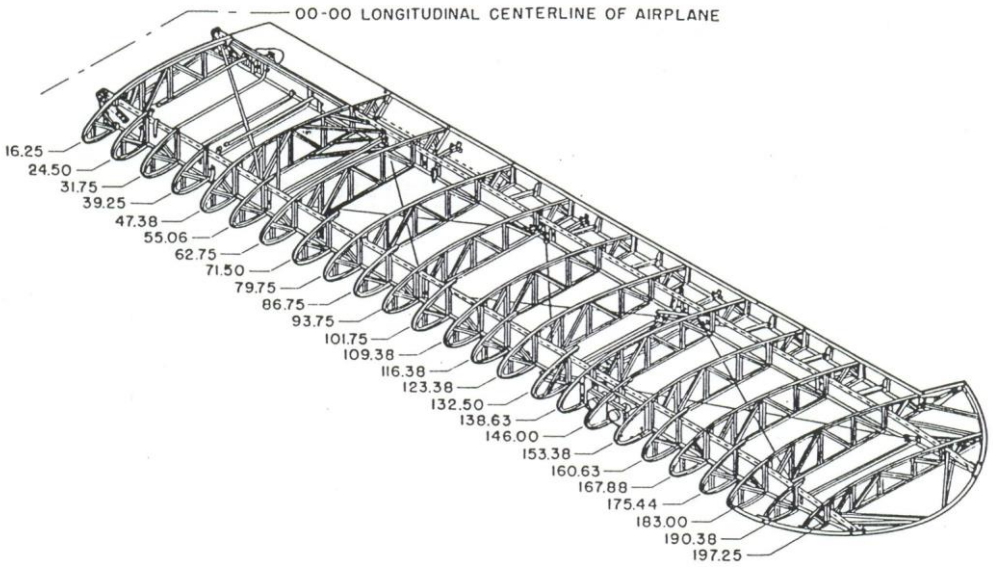

Figure X2–2 PA-18 trussed wing structure [3]

The structure to be sized is given on figure X2–3. The blue shape shown is the right wing of the aeroplane in the structural plane, with the details of the drag truss. Full lines are metal members and dashed lines are wires. Each truss element is numbered for easy reference. The wing has a span of 35 feet, i.e. 420 inches[1], so the wing tip is at WBL 210. Although the root is structurally located at WBL 16, it is aerodynamically located at WBL 12: the air load applied on the skin must be resisted by the inner structure, and the skin extends outwards in all directions. As shown here, the wing plane as a dihedral angle of 3° and a set angle of incidence with respect to the fuselage, as the rear spar is fixed 0.5 in below the front spar.

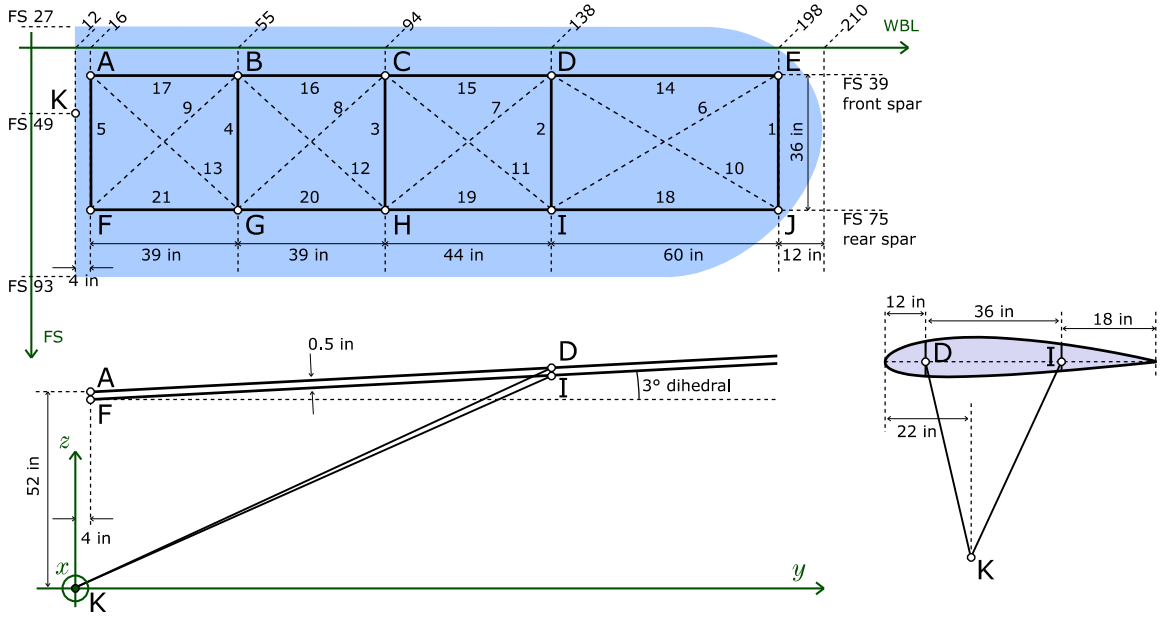

Figure X2–3 PA18 redesign - simplified structural layout

[1] There are 12 inches in one foot.

Global performance data has been computed in a previous application (PA18 redesigned flight envelope). The following figures apply:

- maximum take-off weight: $W_{TO} = 1500$ lbs ;
- nominal stall speed, $V_{st} = 21$ m/s = 40 kts ;
- manoeuvring speed, $V_A = 45$ m/s 85 kts ;
- design cruising speed, $V_C = 50$ m/s = 95 kts ;
- design diving speed, $V_D = 68$ m/s = 132 kts;
- load factor range, 4.5 to −1.8 ;
- aerodynamics, NACA 23015 aerofoil section ;
- aerofoil lift curve: lift coefficient at zero incidence, 0.1 ;
- aerofoil lift curve: linearized slope coefficient, $a_0 = 5.73$ /rad ;
- wing lift curve: linearized slope coefficient, $a = 4.49$ /rad ;
- wing span: $b = 35$ ft ;
- wing area (estimated from drawing): $S = 185$ ft^2 = 17.19 m^2 ;
- wing chord (estimated from drawing): $c = 66$ in = 1.68 m .

Our goal is to find the loads in all structural members shown for the V_A flight condition.

2 Load computation

The manoeuvring speed case corresponds to stall at maximal positive load factor. Since $n^+ = 4.5$, the lift force corresponds to

$$L = 4.5\ W = 6750 \text{ lbs} . \tag{X2.1}$$

The dynamic pressure at V_A is

$$q = \frac{1}{2} \rho\ V_A^{\ 2} = 1240 \text{ Pa} \tag{X2.2}$$

at sea-level conditions. The corresponding lift coefficient can be derived from the lift equation in SI units,

$$C_L = \frac{2\ L}{\rho\ V_A^{\ 2}\ S} = 1{,}41 . \tag{X2.3}$$

This is close to the maximal coefficient used during envelope calculations (there was some round-off carried out in the stall speed).

We shall require a value of angle of attack for later reference. Aerofoil data (see figure X2–4) give the aerofoil lift curve (see determination of the envelope for details):

$$C_L = 5.73\ \alpha + 0.1 = 5.73\ (\alpha + 1.745\ 10^{-2}) . \tag{X2.4}$$

The zero-lift angle of attack is not affected by the finite span, so it remains the same in the wing lift equation. However, the slope of the curve is affected by the finite span (the value has been computed along with the envelope and is given in the data presented above). Hence, the wing lift curve is

$$C_L = 4.49\ (\alpha + 1.745\ 10^{-2}) = 4.49\ \alpha + 0.0783 . \tag{X2.5}$$

This equation can then be used to obtain the angle of attack at stall, i.e.

$$\alpha = \frac{C_L - 0.0783}{4.49} = 0.2966 \text{ rad} = 17° \,. \tag{X2.6}$$

The pitching moment coefficient of the aerofoil is -0.006, yielding a moment of

$$M = \frac{1}{2}\rho\, V_A^{\,2}\, S\, c\, C_m = -214.4 \text{ N}\cdot\text{m} = -1897 \text{ lb}\cdot\text{in} \,, \tag{X2.7}$$

the negative value indicating a nose-down pitching motion.

The drag force is less easy to estimate. First, the induced drag can be obtained from the drag polar equation. Oswald's efficiency of a J-3 Cub (precursor of the PA-18) is quoted to be 0.75 [4]. The aspect ratio (b^2/S) is 6.62, hence

$$C_{D_i} = \frac{C_L^{\,2}}{\pi\, \text{AR}\, e} = 0.1275 \,. \tag{X2.8}$$

Then, the friction drag can be estimated from the profile data with a very crude approach. Considering elliptical loading conditions, the lift coefficient of wing is equal to that of the aerofoil. Figure X2–4 shows the aerodynamic characteristics of a NACA 23015 aerofoil from the classical NACA report 824 by Abbott, von Doenhoff & Stivers [5]. Using a lift coefficient of 1.4 and a Reynolds number of 6 million, the friction drag coefficient is about 0.0133 – a conservative estimate, because non-elliptic loading will tend to increase the induced angle of attack, decreasing the local lift coefficient. Anyway, at high angle of attack conditions, corresponding to low flight speeds, most of the drag is due to the induced drag contribution.

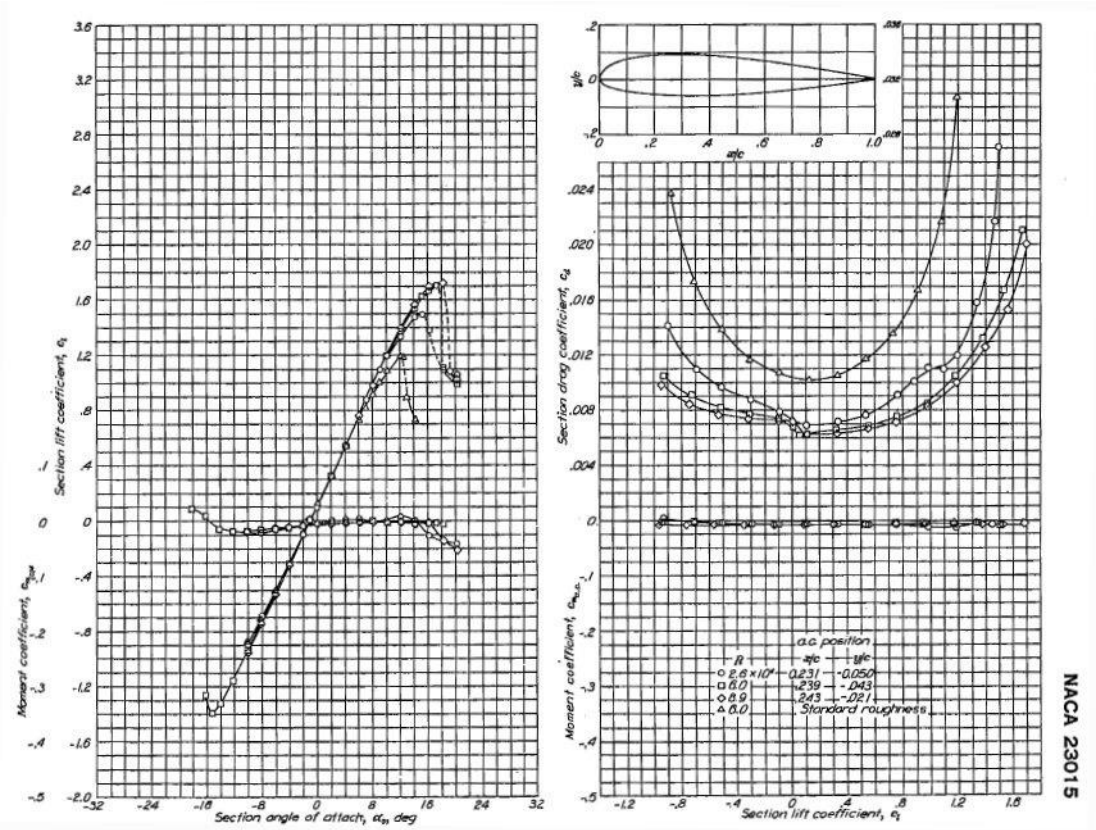

Figure X2–4 Aerodynamic coefficients of the NACA 23015 aerofoil

Finally, the drag force is found to be

$$D = \frac{1}{2}\rho\, V_A^{\,2}\, S\, (C_{D_i} + C_{D_v}) = 3001 \text{ N} = 675 \text{ lb}\,. \tag{X2.9}$$

Now that the aerodynamic forces have been computed, they have to be expressed in the structure-specific frame of reference, which is related to the "normal" and "axial" (or tangent) components with respect to the body-fixed frame rather than the velocity-fixed (or wind-fixed) aerodynamic frame (see figure X2–5). The relations are easily derived using rotation formulas or basic trigonometry; we obtain

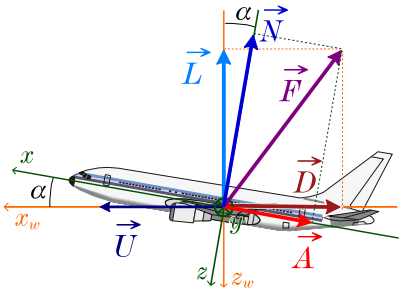

Figure X2–5 Decomposition of air loads in wind and body axes

$$\begin{cases} N = L\cos\alpha + D\sin\alpha = 6652.4 \text{ lbs} \\ A = -L\sin\alpha + D\cos\alpha = -1328.0 \text{ lbs} \end{cases}. \tag{X2.10}$$

As can be seen, the axial force is negative, meaning it is pointing forward, and not backwards (as usually pictured since corresponding to "drag"). This effect, sometimes called "antidrug", is due to the high angle of attack, which casts the lift quite forward of the normal axis. Therefore, even if there is a tendency to call "lift" the normal force and "drag" the tangent force, this example shows us they are not …

3 Structural external loads

The global air loads have been computed in the previous section. They should normally be balanced with inertia loads, but in the present case we have no knowledge of mass distribution, so we will consider air loads only.

Converting global air loads to distributed air loads along the span requires at least a lifting line analysis, which is beyond the scope of this course. As a first estimate, we can approximate the "lift" distribution as sketched on figure X2–6: a constant distribution of intensity q over the span covered by the strut and a linearly-decreasing distribution beyond the strut ends, with an end value of $q/2$. The fuselage provides some lift as well, estimated to be a constant $q/2$.

The "drag" distribution will be assumed to be constant, but over the physical wing span only (since the fuselage does not contribute to the wing drag). The pitching moment should be taken constant along the wing as well.

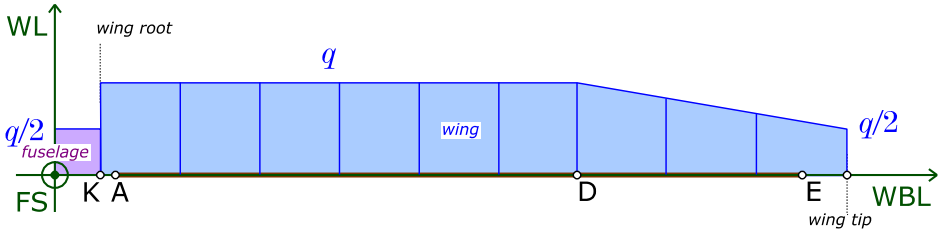

Figure X2–6 Assumed lift distribution

Referring to figure X2–3 for lengths and balancing half of the lift with the assumed distribution, one gets

$$3326.2 = 12\ (q/2) + q\ (4 + 39 + 39 + 44) + 0.5\ (60 + 12)\ (q + q/2)\ , \qquad \text{(X2.11)}$$

yielding

$$q_L = 18.0 \text{ lb/in} \qquad \text{(X2.12)}$$

with a bit of round-up. The values of drag and pitching moment are averaged over a length of 396 in (span without fuselage), yielding

$$q_D = -\ 3.35 \text{ lb/in} \qquad \text{(X2.13)}$$

and

$$q_m = -\ 4.80 \text{ lb} \cdot \text{in/in}\ . \qquad \text{(X2.14)}$$

These loads are supposed to apply at the aerodynamic centre, located at 0.239 of the chord, i.e. 18.8 in from the leading edge. $66 \times 0{,}239 = 15{,}7$??

4 Load transfer into the structure – lift force

The values defined by relations (12) – (14) represent the external load distributions to be applied on the structure. They need to be transferred into the internal structure, which is made up of the main spars, the drag truss and the supporting struts. The proposed methodology involves using superposition of forces to split the analysis between the lift force (normal to the wing plane) and the drag force (tangent to the wing plane).

This part deals with the effect of the lift and moment distributions.

4.1 Equivalent distributed loads on the spars

The load, as computed above, is expressed as reduced at the aerodynamic centre ac. However, the main structural elements which are capable of taking this load are two independent beams: the front and rear spars. Physically, pressure forces pull on the external skin, the skin pulls on the ribs and the ribs pull on the spars, so these forces are physically applied on both spars. There is no moment involved in this structural reduction.

Figure X2–7 shows the lift force system as reduced at the aerodynamic centre and its equivalent reduction as two localized forces on the spars. Note that all loads ($\vec{l}$, $\vec{m}$, $\vec{f}$ and $\vec{b}$) are "running" loads – forces [lb/in] or moments [lb · in/in] spread along the span.

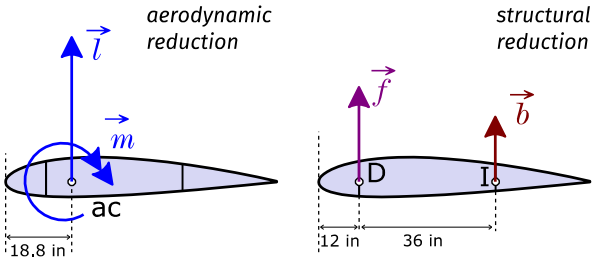

Figure X2–7 Equivalence between loads at the aerodynamic centre and loads applied on the spars

Equivalence implies that the force resultant is the same in both reductions, so

$$l = f + b \tag{X2.15}$$

and it also implies that the moment resultant about any arbitrary point is the same in both reductions, so, using the nose as a reference point,

$$l\, d_l - m = f\, d_f + b\, d_b\,, \tag{X2.16}$$

where d's are corresponding distances from the nose. This set of two equations can be easily solved to yield the intensities of the distributions in the spars.

At any section inwards of D/I, we have

$$\begin{cases} f + b = 18 \\ 12\, f + 48\, b = 18 \times 18.8 - 4.8 \end{cases}. \tag{X2.17}$$

The solution is $f = 14.47$ lb/in and $b = 3.53$ lb/in.

At any section outwards of D/I, the lift load decreases linearly to a tip value of 9. The system written for the tip E/J section is thus

$$\begin{cases} f + b = 9 \\ 12\, f + 48\, b = 9 \times 18.8 - 4.8 \end{cases}, \tag{X2.18}$$

which solution is $f = 7.17$ lb/in and $b = 1.83$ lb/in.

4.2 Global reactions to front spar loading

The loading on the front spar can be summarized as shown on figure X2–8. The running loads, computed from the solution of systems (17) and (18), are balanced by "reacting" forces where the spar is supported, i.e. at points A (fuselage) and D (strut and connecting rod to rear spar). The distributed load is responsible for two different types of loads:

- a transverse load creating a bending moment and shear force in the spar,
- a concentrated action on joint D creating in-plane forces acting on the drag truss, as well as a tensile force in the supporting strut.

This part of the analysis focuses in the concentrated action on joint D.

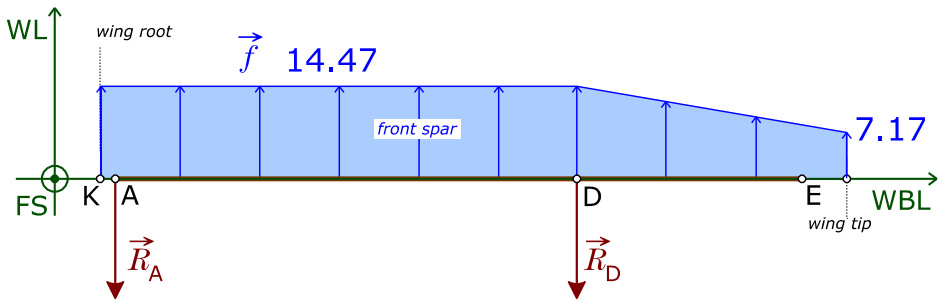

Figure X2–8 Front spar equilibrium between distributed load and joint reactions

Support reactions at A and D can be computed by force and moment equilibrium. In order to do so easily, we can replace the distributed force by three concentrated equivalent contributions, as shown on figure X2–9:

- a resultant $\vec{R}_1$ of the uniform distribution of 14.47 lb/in over 126 in, i.e. 1823.22 lb, applied in the middle of the distribution,
- a resultant $\vec{R}_2$ of the uniform distribution of 7.17 lb/in over 72 in, i.e. 516.24 lb, applied in the middle of the distribution,
- a resultant $\vec{R}_3$ of the triangular distribution of maximal value 7.3 lb/in over 72 in, i.e. 262.80 lb, applied at the inner third of the distribution from the base.

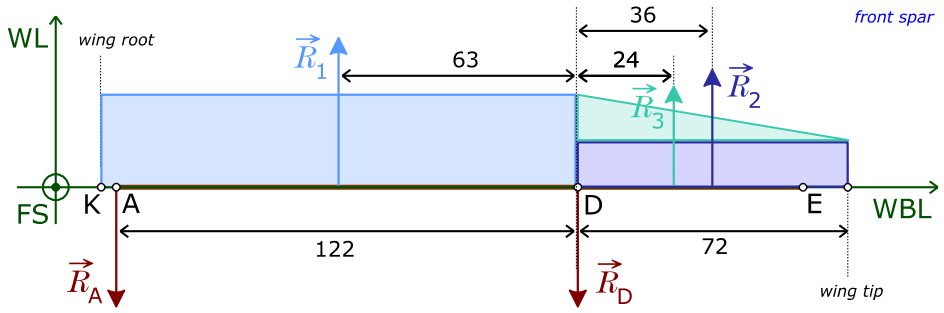

Figure X2–9 Concentrated forces equivalent to the distributed force on the front spar

Moment equilibrium around point D, positive counter-clockwise, then yields

$$122\,R_A - 63\,R_1 + 36\,R_2 + 24\,R_3 = 0\,, \qquad \text{(X2.19)}$$

so

$$R_A = \frac{63\,R_1 - 36\,R_2 - 24\,R_3}{122} = 737{,}47 \text{ lb}\,. \qquad \text{(X2.20)}$$

Force equilibrium then yields R_D:

$$R_D = R_1 + R_2 + R_3 - R_A = 1864.79 \text{ lb}\,. \qquad \text{(X2.21)}$$

These are "abstract" values in the sense that the direction of the reaction forces does not match any physical member in the wing. They represent what the supporting structure has to generate in terms of forces to keep the wing in equilibrium. Conversely, their opposites represent the action that the external lift forces exert on the underlying structure.

4.3 Physical reactions to front spar loading

The force $\vec{R}_D$ is acting on joint D of three-dimensional truss structure. It needs to be transformed into forces resolved along the structural members: as we know from static equilibrium of a two-force system, each rod in a truss must be acted by equal and opposite forces aligned with the rod. This force must then be decomposed into force components along the strut and the truss members. We can do this by applying $\vec{F}_D = -\vec{R}_D$ on joint D as an action force and computing the physical components as reactions required to

maintain equilibrium. $\vec{F}_D$ is nothing else than the action that the lift force causes on joint D, which must be resisted by rod members to maintain equilibrium. Figure X2–10 shows the situation in 3D.

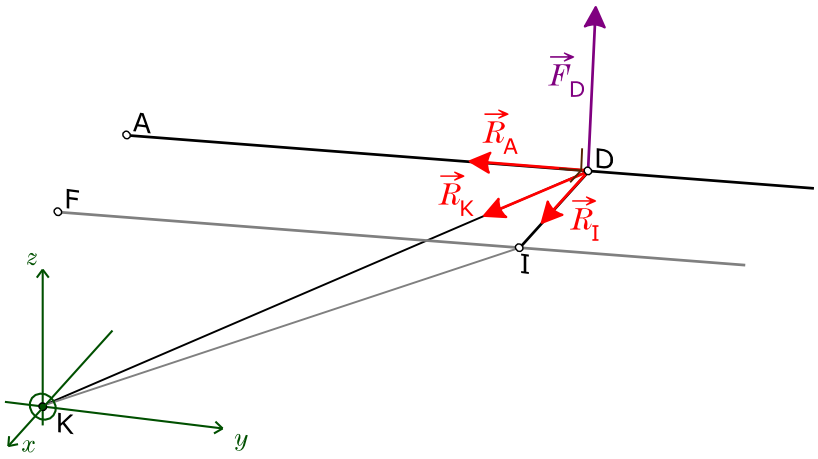

Figure X2–10 Force equilibrium around joint D

The directions of all four forces are not aligned with the global aircraft frame. Therefore, if writing down the vector equilibrium

$$\vec{F}_D + \vec{R}_A + \vec{R}_K + \vec{R}_I = \vec{0} \tag{X2.22}$$

is extremely easy, projecting the equations along the axes of the frame is much more complicated and requires some vector algebra to be carried out easily.

As a prerequisite to those calculations, a table of coordinates for the points seen on figure 10 can be established, keeping in mind the 3° dihedral angle of the spars and the 0.5 shift in the y-direction between the front and rear spars. The coordinates are given in table X2–1, using K as the origin.

Point	x [in]	y [in]	z [in]
A	− 10.00	4.00	52.00
D	− 10.00	125.83	58.38
F	26.00	4.00	51.50
I	26.00	125.83	57.88
K	0.00	0.00	0.00

Table X2–1 Coordinates of major truss joints

Once the coordinates have been determined, it is a simple matter to compute unit vectors along DA, DI and DK (respectively $\vec{e}_A$, $\vec{e}_I$ and $\vec{e}_K$). The procedure for $\vec{e}_A$, for instance, is

$$\vec{e}_A = \frac{(x_A - x_D, y_A - y_D, z_A - z_D)}{\sqrt{(x_A - x_D)^2 + (y_A - y_D)^2 + (z_A - z_D)^2}} \ . \tag{X2.23}$$

The direction of the applied force $\vec{F}_D$ is perpendicular to the plane of the wing. The unit vector corresponding to this direction is obtain by forming a suitable vector product,

$$\vec{e}_\perp = \vec{e}_I \times \vec{e}_A , \qquad \text{(X2.24)}$$

which components can be readily computed with the determinant rule.

Results of these calculations are given in table X2–2.

	cos to x	cos to y	cos to z
$\vec{e}_A$	0.0000	− 0.9986	− 0.0523
$\vec{e}_I$	0.9999	0.0000	− 0.0139
$\vec{e}_K$	0.0719	− 0.9048	− 0.4198
$\vec{e}_\perp$	0.0139	− 0.0523	0.9985

Table X2–2 Direction cosines for all directions relevant to joint D equilibrium

Equation (22) can now be projected along the three axes of the reference frame, yielding the following system of equations:

$$\begin{cases} 0.0719\, R_K + 0.9999\, R_I = -0.0139\, F_D = -25.9206 \\ -0.9986\, R_A - 0.9048\, R_K = 0.0523\, F_D = 97.53 \\ -0.0523\, R_A - 0.4198\, R_K - 0.0139\, R_I = -0.9985\, F_D = -1861.99 \end{cases} \qquad \text{(X2.25)}$$

which has the solution

$$\begin{cases} R_A = -4653.36 \\ R_K = 5027.98 \\ R_I = -387.47 \end{cases} \text{ [lb] .} \qquad \text{(X2.26)}$$

These values are reactions to the physical "pull" of the force $\vec{F}_D$ on joint D. Hence, the physical actions of $\vec{F}_D$ along the rod members of the truss and along the strut are given by opposite forces, i.e. values with reversed signs. Figure X2–11 shows the physical direction of all three physical actions caused by the lift force distribution on the front spar acting at joint D on the drag truss and front strut. Notice how $\vec{F}_K$ pulls on the strut. Regarding $\vec{F}_A$ and $\vec{F}_I$, their intensity is negative after the reversal operation, so the direction of those forces is reversed a second time to show the physical direction of action. As we see, $\vec{F}_A$ puts the front spar in compression and $\vec{F}_I$ puts the rib between the spars in compression as well. Force $\vec{F}_A$ and $\vec{F}_I$ are to be understood as "external" forces acting on the in-plane drag truss. Force $\vec{F}_K$ is the "external" force acting on the strut; it directly corresponds to the tensile force in strut DK (two-force member).

The same procedure must be carried over a second time in order to resolve the loads caused by the forces on the rear spar.

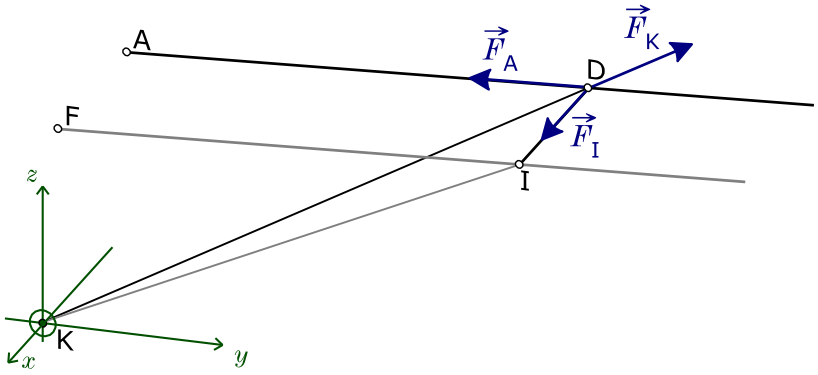

Figure X2–11 Physical actions of the lift distribution on the front spar applied on joint D

4.4 Global reactions to rear spar loading

Figure X2–12 shows the distributed action reduced on the rear wing. This load is equilibrated by reactions from joints F and I in a plane perpendicular to the wing.

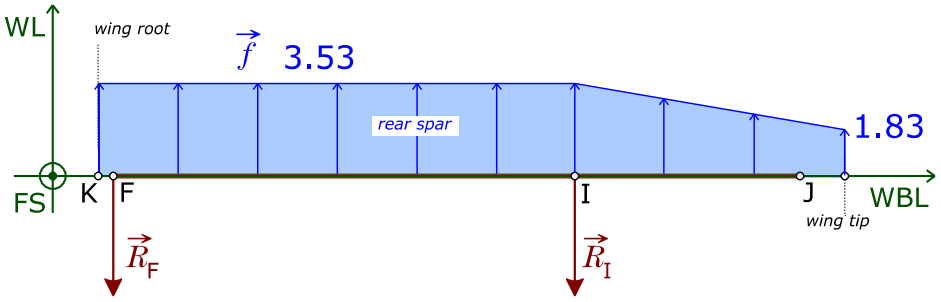

Figure X2–12 Rear spar equilibrium between distributed load and joint reactions

We can use the same approach we already used (see figure X2–9). The intensities are now $R_1 = 444.78$ lb, $R_2 = 131.76$ lb, $R_3 = 61.2$ lb, $R_F = 178.76$ lb and $R_I = 458.98$ lb.

4.5 Physical reactions to rear spar loading

Figure X2–13 shows the physical equilibrium at joint I between the pull on the joint by the lift force and the reactions along the truss members. The equilibrium equation is resolved by the same procedure as already used on joint D. From the coordinates of table X2–1 we can generate direction cosines for all directions implied in the equilibrium. They are summarized in table X2–3. The resulting system of equations has the solution

$$\begin{cases} R_D = -225.03 \\ R_F = -1145.42 \text{ [lb]} \\ R_K = 1254.12 \end{cases} . \qquad \text{(X2.27)}$$

The physical actions caused on the drag truss and rear strut are obtained by inverting the direction (action/reaction) and inverting again the forces with negative intensities. The results are shown on figure X2–14.

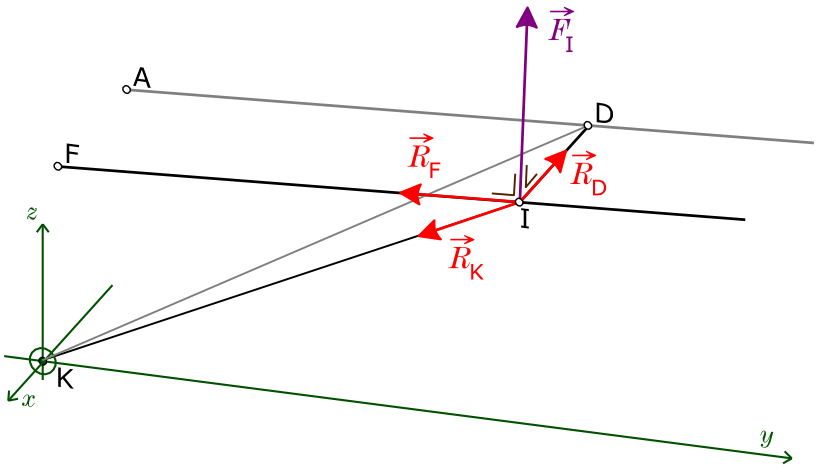

Figure X2–13 Force equilibrium around joint I

	cos to x	cos to y	cos to z
$\vec{e}_D$	− 0.9999	0.0000	0.0139
$\vec{e}_F$	0.0000	− 0.9986	− 0.0523
$\vec{e}_K$	− 0.1845	− 0.8929	− 0.4107
$\vec{e}_\perp$	0.0139	− 0.0523	0.9985

Table X2–2 Direction cosines for all directions relevant to joint I equilibrium

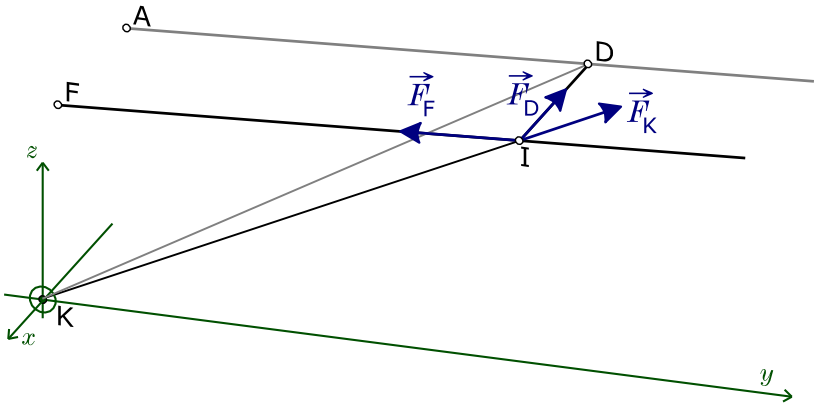

Figure X2–14 Physical actions of the lift distribution on the rear spar applied on joint I

5 Load transfer into the structure – drag force

The “drag” force is acting forward. Since the joints are pinned in the plane of the wing, is may be safely assumed that the wing “pushes” the ribs forward, which in turn act on the rear strut forward. Hence, the distributed drag force is to be distributed on the joints of the rear strut.

The equilibrium problem can be thought of as represented on figure X2–15 but this is really an equivalence problem: the spar itself being hinged, it would not be in equilibrium in that case: in reality the spar does not move because it is part of the drag truss, which is rigid. The purpose

of this analysis is to reduce the drag load to the individual joints by ensuring equivalence of force and moment.

The problem is apparently indeterminate, but can be solved approximately by using reasonable assumptions. First, $\vec{R}_G$ stands in between 2 segments of equal length, so it is reasonable to assume

$$R_G = 39 \times 3.35 = 130.65 \text{ lb} . \tag{X2.28}$$

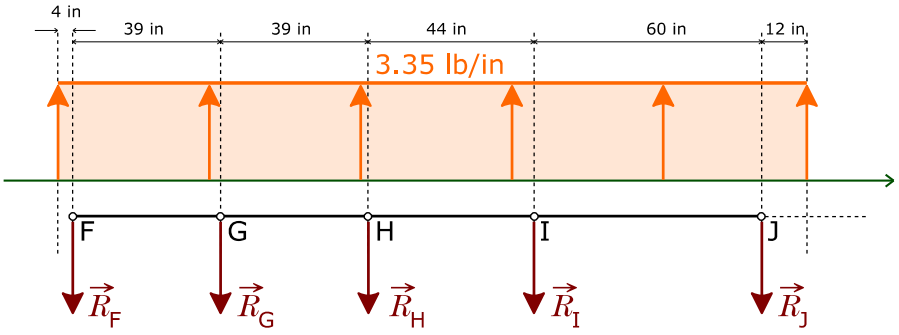

Figure X2–15 Equivalence between applied drag force and drag actions on the drag truss

Then, cutting at G and I to isolate the two outer segments (see figure X2–16), we can express equivalence of each distribution with each reaction through a moment equilibrium around the inner joints, respectively G and I, to cancel out reactions at G and I. By this technique, we can obtain values of $\vec{R}_F$ and $\vec{R}_J$ which respect moment equilibrium of these outer segments.

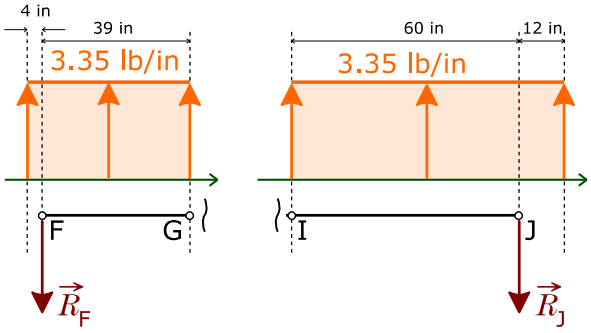

Figure X2–16 Equivalence for the inner and outer segments

For joint F, equilibrium about G yields

$$R_F = \frac{(43 \times 3.35) \times 21.5}{39} = 79.41 \text{ lb} , \tag{X2.29}$$

while equilibrium about I yields

$$R_J = \frac{(72 \times 3.35) \times 36}{60} = 144.72 \text{ lb} . \tag{X2.30}$$

We are then left with two unknowns, which can be set to satisfy global force and moment equilibrium.

$$R_H + R_I = 198 \times 3.35 - 130.65 - 79.41 - 144.72 = 308.52 \tag{X2.31}$$

and

$$82\, R_H + 126\, R_I = 198^2 \times 3.35/2 - 130.65 \times 43 - 79.41 \times 4 - 144.72 \times 186$$
$$= 32813.19 . \tag{X2.32}$$

Moment equilibrium

The solution of this system of two equations in two unknowns is

$$\begin{cases} R_H = 137.73 \\ R_I = 170.79 \end{cases} \text{[lb]} \ . \tag{X2.33}$$

This completes the resolution of the drag force into individual forces applied on the truss through the joints.

6 Drag truss solution

At this point, the drag truss can be solved. The final distribution of external forces on the truss is given on figure X2–17: the blue forces $\vec{X}_D$ and $\vec{Y}_D$ correspond to the actions on joint D from the applied lift, the blue forces $\vec{X}_I$ and $\vec{Y}_I$ correspond to the actions on joint I from the applied lift, and the orange forces $\vec{D}_F$ through $\vec{D}_J$ correspond to the actions on joints F through J from the applied drag. Reaction forces from the fuselage are of course added for equilibrium. F is assumed to be the sliding joint. The values of the loads are summarized in table X2–4.

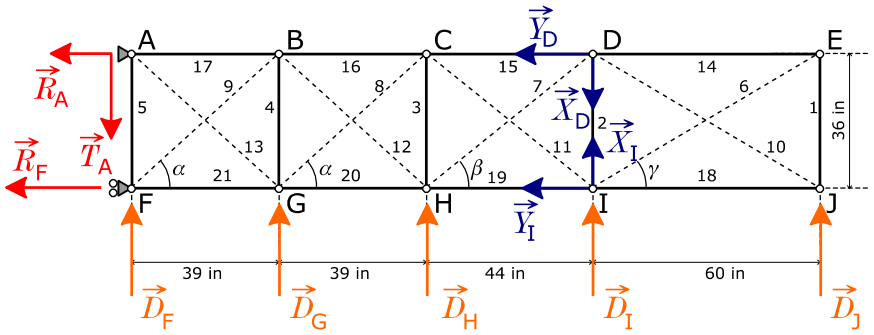

Figure X2–17 Drag truss with external forces (loads and in-plane reactions)

Action of lift	Value [lb]	Action of drag	Value [lb]
X_D	387.47	D_F	79.41
Y_D	4653.36	D_G	130.65
X_I	225.03	D_H	137.73
Y_I	1145.42	D_I	170.79
		D_J	144.72

Tableau X2–4 Summary of external forces applied on the drag truss

The computation of the truss requires knowledge of the angles in the truss bays. From simple trigonometry, we find

$$\alpha = 42.71° \ , \tag{X2.34}$$

$$\beta = 39.29 \ °, \tag{X2.35}$$

$$\gamma = 30.96° \ . \tag{X2.36}$$

Although this is a simple triangulated truss which can be computed using the method of joints, an added difficulty lies in the wired diagonal members; one has to determine in advance which is under tension and which is under compression within a bay (it must be one or the other). Unless one has a developed structural feeling, this can simply be managed by trial-and-error.

A priori, considering drag forces only, the truss is "pushed up", so diagonals 6 through 9 should be under tension. We can then start the truss analysis at joint J, since there will be only two unknowns at the joint, making it solvable through joint equilibrium. Cutting around the joint "exteriorizes" the internal stress resultant in truss members 1 and 18, see figure X2–18. Denoting those internals $\vec{N}$, we obtain the system

$$\begin{cases} N_{18} = 0 \\ N_1 + D_J = 0 \end{cases} \tag{X2.37}$$

which yields

$$\begin{cases} N_1 = -144.72 \text{ lb} \\ N_{18} = 0 \end{cases}. \tag{X2.38}$$

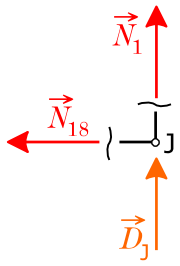

Figure X2–18 Equilibrium of joint J

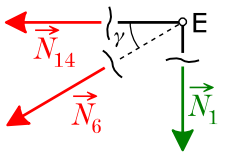

Figure X2–19 Equilibrium of joint E

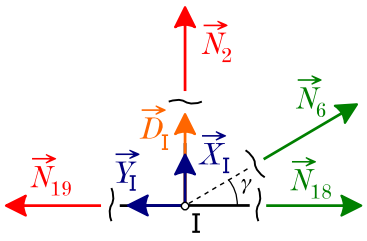

Figure X2–20 Equilibrium of joint I

We can then move on to joint E (X2–19. Internal stress resultant $\vec{N}_1$ is known from the previous step so it is drawn in green (note that the force was reversed since we are now looking at the other end of the rod member; its numerical value is negative, in accordance with result 38). Equilibrium relations are thus written

$$\begin{cases} N_{14} + N_6 \cos\gamma = 0 \\ N_1 + N_6 \sin\gamma = 0 \end{cases}, \tag{X2.39}$$

yielding

$$\begin{cases} N_6 = 281.32 \text{ lb} \\ N_{14} = -241.24 \text{ lb} \end{cases}. \tag{X2.40}$$

As we can see, the value of N_6 positive, which means that the wire is undergoing tension, as supposed earlier.

The next joint in the sequence is joint I (figure X2–20). The equilibrium implies more forces, since new external forces are brought into the truss at joint I:

$$\begin{cases} N_{18} + N_6 \cos\gamma - N_{19} - Y_I = 0 \\ N_2 + N_6 \sin\gamma + X_I + D_I = 0 \end{cases}. \tag{X2.41}$$

The solution of the system is

$$\begin{cases} N_2 = -540.54 \text{ lb} \\ N_{19} = -904.18 \text{ lb} \end{cases} . \tag{X2.42}$$

Stepping to joint D (figure X2–21), we have the following equilibrium

$$\begin{cases} N_{15} + N_7 \cos\beta - N_{14} + Y_D = 0 \\ N_2 + N_7 \sin\beta + X_D = 0 \end{cases} \tag{X2.43}$$

giving the solution

$$\begin{cases} N_7 = 241.72 \text{ lb} \\ N_{15} = -5081.68 \text{ lb} \end{cases} . \tag{X2.44}$$

This result confirms that wire 7 is under tension.

Moving to joint H (figure X2–22),

$$\begin{cases} N_{20} - N_7 \cos\beta - N_{19} = 0 \\ N_3 + N_7 \sin\beta + D_H = 0 \end{cases} \tag{X2.45}$$

and

$$\begin{cases} N_3 = -290.80 \text{ lb} \\ N_{20} = -717.10 \text{ lb} \end{cases} . \tag{X2.46}$$

Moving next to joint C (figure X2–23), we obtain

$$\begin{cases} N_{16} + N_8 \cos\alpha - N_{15} = 0 \\ N_3 + N_8 \sin\alpha = 0 \end{cases} , \tag{X2.47}$$

leading to

$$\begin{cases} N_8 = 428.73 \text{ lb} \\ N_{16} = -5396.71 \text{ lb} \end{cases} . \tag{X2.48}$$

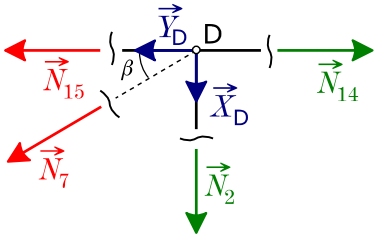

Figure X2–21 Equilibrium of joint D

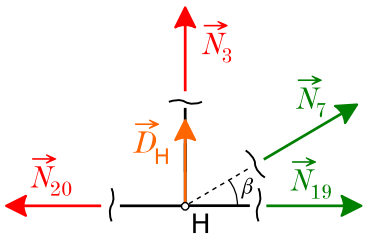

Figure X2–22 Equilibrium of joint H

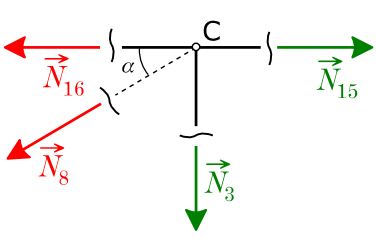

Figure X2–23 Equilibrium of joint C

Joint G (figure X2–24) is similar to joint H:

$$\begin{cases} N_{21} - N_8 \cos\alpha - N_{20} = 0 \\ N_4 + N_8 \sin\alpha + D_G = 0 \end{cases} \tag{X2.49}$$

and

$$\begin{cases} N_4 = -421.45 \text{ lb} \\ N_{21} = -402.34 \text{ lb} \end{cases} . \tag{X2.50}$$

Joint B (figure X2–25) is similar to joint C:

$$\begin{cases} N_{17} + N_9 \cos\alpha - N_{16} = 0 \\ N_4 + N_9 \sin\alpha = 0 \end{cases} \tag{X2.51}$$

and

$$\begin{cases} N_9 = 621.34 \text{ lb} \\ N_{17} = -5853.27 \text{ lb} \end{cases} . \tag{X2.52}$$

Now we reach the fuselage. The drag truss is normally fitted in a statically determined way, i.e. with one sliding joint in the drag direction. Let us assume the sliding joint is F. Then, the only reaction is the spanwise component $\vec{R}_F$, see figure X2–26. The equilibrium relations are

$$\begin{cases} R_F - N_9 \cos\alpha - N_{21} = 0 \\ N_5 + N_9 \sin\alpha + D_F = 0 \end{cases} , \tag{X2.53}$$

yielding

$$\begin{cases} N_5 = -500.86 \text{ lb} \\ R_F = 54.22 \text{ lb} \end{cases} . \tag{X2.54}$$

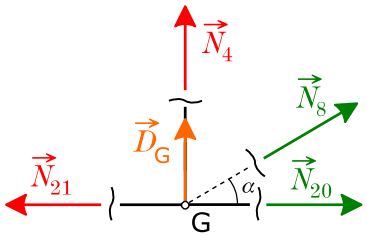

Figure X2–24 Equilibrium of joint G

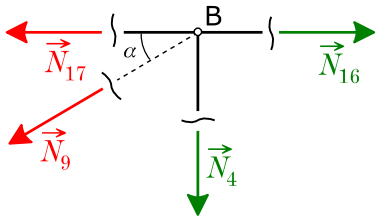

Figure X2–25 Equilibrium of joint B

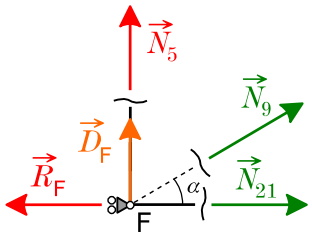

Figure X2–26 Equilibrium of joint F

Finally, we move to joint A. Figure X2–27 shows the equilibrium diagram. All tensile/compressive internal stress resultant forces have now been computed. There only remain the reactions from the fuselage at joint A. Here we have both a spanwise reaction $\vec{R}_A$ but also a reaction $\vec{T}_A$ in a direction tangent to the plane of the wing since joint A is not allowed to slide like joint F, so as to fix the wing in its plane.

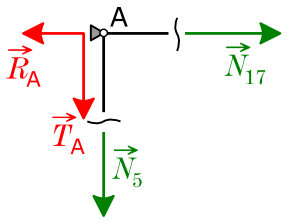

Figure X2–27 Equilibrium of joint A

The final equations are

$$\begin{cases} R_A - N_{17} = 0 \\ N_5 + T_A = 0 \end{cases} , \tag{X2.55}$$

which have the solution

$$\begin{cases} R_A = -5853.27 \text{ lb} \\ T_A = 500.86 \text{ lb} \end{cases} . \tag{X2.56}$$

Referring again to figure X2–17, a sure way to cross-check the truss calculation is to compute the equilibrium in spanwise and axial directions along the wing surface. This gives

$$Y_D + Y_I + R_A + R_F = -0.27 \approx 0 \tag{X2.57}$$

and

$$D_F + D_G + D_H + D_I + D_J + X_I - X_D - T_A = 0.00 , \tag{X2.58}$$

showing that global equilibrium is satisfied.

7 Transfer of loads at the fuselage

The full computation also provides all loads transferred to the fuselage by the wing – they just need to be collated from where in the development they have been computed. Figure X2–28 shows the forces applied to the fuselage by the wing: they are essentially the opposite of the various reactions computed throughout this case.

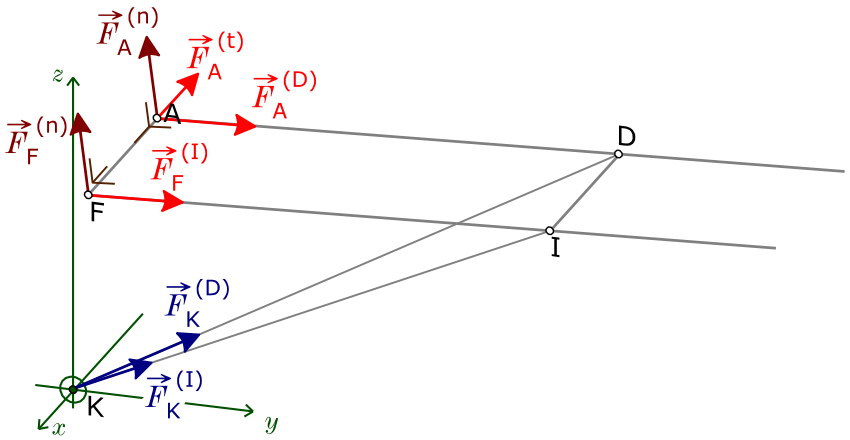

Figure X2–28 Individual loads transferred to the fuselage at the supporting joints

7.1 Strut base (joint K)

Joint K is subject to tensile forces along KD and KI, corresponding to the $\vec{F}_K$ forces from sections 4.3 and 4.5. The direction cosines can be obtained from tables X2–2 and X2–3 (note that signs have been reversed since the positive direction for the load on the fuselage is from K to D or from K to I), allowing to obtain the force components along the fuselage global frame. Details of the computation are given in table X2–5.

7.2 Rear spar end (joint F)

Joint F is subject to the spanwise action from the drag truss and the pull from the lift force distributed on the rear spar, acting normal to the plane of the wing. using the appropriate direction cosines and magnitudes, we obtain the load transfer through table X2–6.

7.3 Front spar end (joint A)

Finally, joint A is treated in a similar fashion; however, there is an additional action to be considered here as joint A takes the axial thrust created by the anti-drag force in the wing plane. It is the inverse of reaction $\vec{T}_A$ and is labelled $\vec{F}_A^{(t)}$ in figure X2–28. Results for the force components are summarized in table X2–7.

7.4 Final cross-check: global equivalence with air loads

As a final verification of the accuracy, let us note that the original air loads are supposed to be equivalent to the total actions on the fuselage. It is possible to verify this by summing the air loads and projecting in the global frame.

The total "lift" is 3240 lb (up), the total "drag" is 664 lb (forward). Table X2–8 shows the force components in the global frame. The line ***external load total*** indicates the total resultant components. The line ***fuselage load total*** contains the sum of the force components applied at joints A, F and K. As the table shows, the accuracy is quite good.

Element	magnitude	cos to x	cos to y	cos to z	F_x	F_y	F_z
$F_K^{(D)}$	5027.98	− 0.0719	0.9048	0.4198	− 361.51	4549.32	2110.75
$F_K^{(I)}$	1254.12	0.1845	0.8929	0.4107	231.39	1119.80	515.07
Joint K					**− 130.12**	**5669.12**	**2625.82**

Table X2–5 Transfer of loads to the fuselage at support point K

Element	magnitude	cos to x	cos to y	cos to z	F_x	F_y	F_z
$F_F^{(n)}$	178.76	0.0139	− 0.0523	0.9985	2.48	− 9.35	178.49
$F_F^{(I)}$	54.22	0.0000	0.9986	0.0523	0.00	54.14	2.84
Joint F					**2.48**	**44.79**	**181.33**

Table X2–6 Transfer of loads to the fuselage at support point F

Element	magnitude	cos to x	cos to y	cos to z	F_x	F_y	F_z
$F_A^{(n)}$	737.47	0.0139	− 0.0523	0.9985	10.25	− 38.57	736.36
$F_A^{(t)}$	500.86	− 0.9999	0.0000	0.0139	− 500.81	0.00	6.96
$F_A^{(D)}$	− 5853.27	0.0000	0.9986	0.0523	0.00	− 5845.08	− 306.13
Joint A					**− 490.56**	**− 5883.65**	**437.19**

Table X2–7 Transfer of loads to the fuselage at support point A

Element	magnitude	cos to x	cos to y	cos to z	F_x	F_y	F_z
$L^{(n)}$	3240	0.0139	− 0.0523	0.9985	45.04	− 169.45	3235.14
$D^{(t)}$	664	− 0.9999	0.0000	0.0139	− 663.93	0.00	9.23
External load total					**− 618.89**	**− 169.45**	**3244.37**
Fuselage load total					**− 618.20**	**− 169.74**	**3244.34**

Table X2–8 Equivalence between external aerodynamic loads and loads as applied to the fuselage

8 Sizing

The purpose of this example is load determination, not actual sizing; however, we can discuss some items related to sizing.

All rod members are subject to tension and compression only. Therefore, rod members under tension can be directly sized by tension theory ($\sigma = N/A$). Rod members under compression can be sized using the same kind of relations provided that they are safe from buckling. This depends on the chosen cross-section and whether it is stable or not.

The spars pose an additional challenge. Although "hinged" at joints D and I, the bending moment is not zero at these joints – otherwise, the outer segments [DE] and [IJ] would obviously "flap up" and rotate. So there must be a bending moment (and shear force) distribution in the spars, which must be taken into account. However, the external bracing drastically reduced the intensity of the maximal bending moment.

9 References

[1] Anon. *Piper J-3 Cub*. Wikipedia, the free encyclopedia.

[2] Anon. *Piper PA-18 Super Cub*. Wikipedia, the free encyclopedia.

[3] Anon. *Piper PA-18 structural drawings*.
(I have unfortunately not kept any details about this reference).

[4] Nita, M. & Scholz, D. *Estimating the Oswald factor from basic aircraft geometric parameters*. Deutscher Luft-und-Raumfahrtkongress 2012, document ID 281424.

[5] Abbott, I.H., von Doenhoff, A.E. & Stivers, L.S.Jr. *Summary of airfoil data*. NACA report 824, 1945.